

Guiding Center Orbit Studies in a Tokamak Edge Geometry Employing Boozer and Cartesian Coordinates

Y. Nishimura*, Y. Xiao, and Z. Lin

Department of Physics and Astronomy, University of California, Irvine, 92697-4575, USA

Received 23 May 2007, accepted 17 November 2007

Published online 18 March 2008

Key words Guiding center orbit, boozer coordinate, tokamak edge geometry, global field aligned mesh.

PACS 52.30.Gz, 52.55.Rk, 52.65.Cc

Guiding center Monte-Carlo codes (GCMC) in both open and closed field line regions in the tokamak edge geometry are developed for the future applications in examining the integration of core and edge turbulence transport simulations. Introducing a simple analytical model for the edge geometry, the orbital studies are presented.

© 2008 WILEY-VCH Verlag GmbH & Co. KGaA, Weinheim

1 Introduction

Various investigations have continued to seek for the origins of the radial electric fields in the tokamak H-modes. [1] Self-consistent gyrokinetic simulations have advantages over fluid type edge turbulence simulations [2, 3] in that they can incorporate three possible mechanisms of the E_r generation, that are the non-ambipolar ion orbital losses, [4] the Reynolds stress, [5] and the balance between perpendicular and parallel currents through the quasi-neutrality condition, [6–8] all simultaneously. For gyrokinetic simulations, computational efficiency is the key. Global field aligned mesh [9] provides us with the highest computational efficiency. In a typical GTC simulation for example, [10] sixty four toroidal planes are employed for the ITER size plasmas while thousands are required for regular mesh to resolve the ion Larmor radius scale in the toroidal direction. Global field aligned mesh has been constructed in the open and the closed field line regions [11, 12] where the gyrokinetic Poisson equation [13, 14] is solved. However, from the guiding center orbit point of view, while the Boozer coordinate [15] can be applied to the closed field line region, one need to employ the Cartesian or cylindrical coordinates [16] in the open field line region where periodicity is not guaranteed. In this work, as a preliminary study to the gyrokinetic turbulence simulation, two guiding center Monte Carlo codes (GCMC) are employed separately for the closed field line region and the open field line region. We develop these tools (with an analytical magnetic field model) for the purpose of examining if connecting the two (in a global field aligned mesh) can be done without losing accuracy at the separatrix. The analytical model is also useful to study subtle transport mechanisms near the X-point. [17, 18] The present studies can facilitate the integration of gyrokinetic codes in tokamak core (GTC, [10] for example) and edge (XGC, [18] for example).

2 The magnetic field and the guiding center model

In this section, the basic properties of a magnetic field representation and the guiding center drift model are briefly reviewed. In the closed field line region we can employ the Boozer coordinate. [15] The Boozer coordinate (ψ, θ, ζ) allows for the poloidal and toroidal covariant components to be only the function of the equilibrium flux surface label. In the Boozer coordinate, the covariant and the Clebsch form of the magnetic field are given by

$$\mathbf{B}_{cov} = G(\psi) \nabla \zeta + I(\psi) \nabla \theta + \delta(\psi, \theta, \zeta) \nabla \psi \quad (1)$$

$$\mathbf{B}_{clebsch} = \nabla \psi \times \nabla(\theta - \zeta/q) \quad (2)$$

*Corresponding author: e-mail: nishimuy@uci.edu

where q is the safety factor.

On the other hand, for the open field line region in the Cartesian coordinate system, we employ an analytical function to generate a tokamak edge like geometry. [12] The model is given by a combination of circles and hyperbolic curves. Although simple, it produces a geometry which is sufficient enough to study important edge turbulence issues. In particular, the model produces the X-point singularity of the divertor separatrix. To describe the magnetic geometry, we consider a Hamiltonian of the form

$$H_h(x, y) = \varepsilon B_0 \left(\frac{y^2}{2} - \frac{x^2}{2} \right) \quad (3)$$

for a domain which satisfies $y \leq x + \sqrt{2}$ and $y \leq -x + \sqrt{2}$ (hyperbolic curves), and circles for the rest of the domain (the magnetic field line pitch is smoothly connected through the $y = \pm x + \sqrt{2}$ boundaries). Here, the inverse aspect ratio is given by ε . The center of the circle is located at $(x, y) = (0, \sqrt{2})$. Equation (3) applies to both the open and the closed field line regions. The singular feature of the X-point is captured in [12]. The magnetic field components in the hyperbolic region are given by $B_x = \dot{x} = \partial_y H = \varepsilon B_0 y$ and $B_y = \dot{y} = -\partial_x H = \varepsilon B_0 x$. We impose the toroidal curvature effect as $B_z = B_0(1 - \varepsilon x)$. Here, B_0 is the toroidal magnetic field strength at the axis.

The equation of motion is time advanced both in the Boozer [15] coordinate (ψ, θ, ζ) and in the Cartesian coordinate (x, y, z) the latter being similar to the infinite cylinder. [16] The guiding center equation by Littlejohn [19] in cgs-Gaussian units is given by

$$\dot{\mathbf{X}} = v_{\parallel} \frac{\mathbf{B}^*}{B_{\parallel}^*} + \frac{c}{qB_{\parallel}^*} \mathbf{b} \times (\mu \nabla B - q \mathbf{E}^*) \quad (4)$$

$$v_{\parallel} = -\frac{\mathbf{B}^*}{mB_{\parallel}^*} \cdot (\mu \nabla B - q \mathbf{E}^*) \quad (5)$$

where \mathbf{X} is the position, v_{\parallel} is the velocity parallel to the equilibrium magnetic field, $\mu = mv_{\perp}^2/2B$ is the magnetic moment. Here, m and q are the mass and the charge of the particles, c is the speed of light. We do not use conventional $e = m = c = 1$ normalization. [19] We would like to differentiate ion and electron dynamics. For the field quantities, $\mathbf{B}^* = \mathbf{B} + (mcv_{\parallel}/q)\nabla \times \mathbf{b}$ ($\mathbf{b} = \mathbf{B}/|B|$), $B_{\parallel}^* = \mathbf{b} \cdot \mathbf{B}^*$, and \mathbf{E}^* includes the induction component on top of the electrostatic one. Note that the \mathbf{B}^* term contains the conventional curvature drift term. In applying Eqs.(4) and (5) to the Cartesian coordinate system with Eq.(3), the phase conserving term [20] (also referred to as Banos drift [21]) is neglected due to the ordering in ε .

Monte Carlo techniques are employed for collision effects. A pitch angle scattering ($\lambda = v_{\parallel}/v$ and $v^2 = v_{\parallel}^2 + v_{\perp}^2$) and an energy scattering is employed. Here, we simulate the Lorentz collision operator [22]

$$C(f) = \frac{\nu}{2} \frac{\partial}{\partial \lambda} \left[(1 - \lambda^2) \frac{\partial}{\partial \lambda} \right]. \quad (6)$$

The algorithm is the one employed in [22]. The test particles change the parallel and perpendicular velocity components by

$$\lambda_{new} = \lambda_{old} (1 - \nu\tau) \pm [(1 - \lambda_{old}^2) \nu\tau]^{1/2} \quad (7)$$

where the ion-ion collision frequency is given by ν , τ is the length of the time between the steps, and the symbol \pm implies the randomness. Likewise, the energy scattering operator is incorporated. [22]

3 Simulation results

Shown in Fig.1(a) is the projection of a guiding center motion of a $3.5(MeV)$ α particle onto a poloidal plane. In Fig.1(a), the guiding center equation is solved in the Boozer coordinate [simply take scalar products of Eq.(4) with $\nabla\psi$, $\nabla\theta$, and $\nabla\zeta$ to obtain the guiding center equation of motion]. A typical large tokamak like parameters are used [$B_0 = 1(T)$, minor radius $1(m)$, and a parabolic profile for the safety factor are taken]. In this example,

the orbit is trapped (exhibits a banana motion). The breaking of the second adiabatic invariant is due to the finite ion-ion collisions (pitch angle scattering) and the ion-electron collisions (energy scattering) where the Monte-Carlo techniques are employed. To gain confidence in the solution of the guiding center orbit following code, diffusion coefficients versus the collision frequency is further estimated (in the Boozer coordinate system). Figure 1(b) shows diffusion coefficients versus the collision frequency obtained from statistical evaluations of the second order cumulants. A total of 1000 particles is employed (as an initial condition of particles, 10 different poloidal locations, 10 toroidal locations, and 10 pitch angles are employed). In Fig.1(b), the enhancement of a diffusive transport is seen in $10^{-6} < \nu/\Omega_c < 10^{-4}$ which corresponds to the Banana regime of the neoclassical transport theory. [15] In Fig.1(b), hydrogen ions with a monochromatic energy of 3.5(keV) are employed.

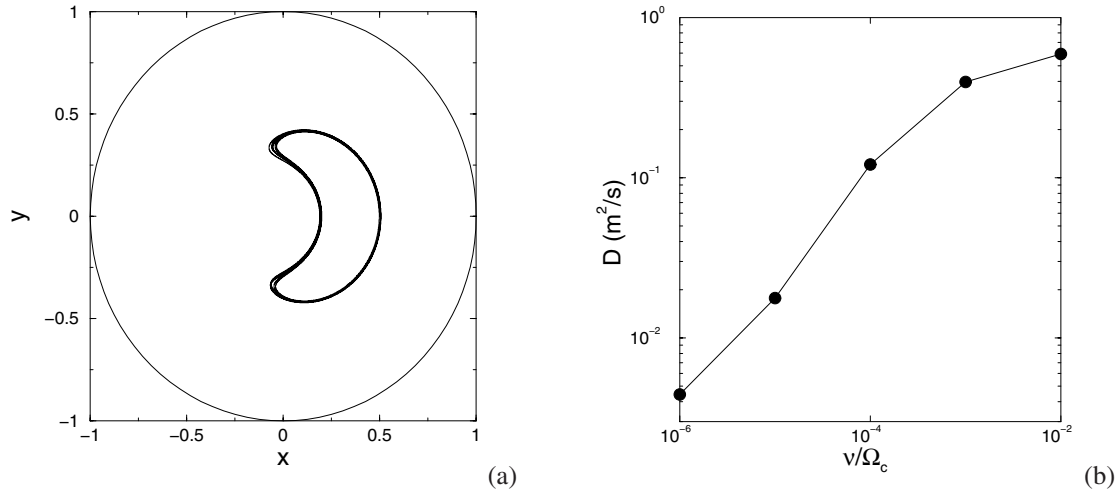


Fig. 1 (a) Two dimensional projection of a guiding center banana orbit in a tokamak. The Boozer coordinate is employed in the orbit following code. Here, $\nu/\Omega_c = 10^{-6}$ is taken. (b) Diffusion coefficient of 3.5(keV) hydrogen ions versus the ion-ion collisionality. The pitch angle scattering operator is employed.

On the other hand, shown in Fig.2 is the projection of guiding center motions of 3.5(keV) hydrogen ions where the guiding center equation is time advanced in the Cartesian coordinate (see Appendix for the equation of motion). For the verification purpose, shown in Fig.2(a) are the guiding center orbits in the absence of toroidal curvature effects ($B = const$) which is equivalent to a magnetic field line Poincare plot. Figure 2(b) shows the orbits inside and outside the separatrix in the presence of the toroidal curvature effect $B = B_0(1 - \epsilon x)$ and with the pitch angle scattering. In this part of the calculation \mathbf{E}^* is set to be zero.

To time advance the equation of motion, both the second order Runge-Kutta method and fourth order Runge-Kutta-Gill method are employed. [23] Compared to the standard algorithm, for example by Abramowitz and Stegun, [24] a better fourth order Runge-Kutta-Gill method can be found which includes corrections to the truncation error [25] (which also has an advantage in saving computational memories). While the examples above employed an analytical magnetic configuration, a bi-cubic spline method has been incorporated in the guiding center orbit following code so that the magnetic components of numerical equilibria of tokamaks can be read in.

4 Summary and discussions

In this work, guiding center orbit following codes are developed and applied to tokamak geometries in the Boozer coordinate and in the Cartesian coordinate. We have employed a simple analytical model for the edge divertor geometry. The analytical model can be useful in the initial phase of the edge code development (compared to numerical equilibria from Grad Shafranov solvers, which may obscure mathematical singularity of the separatrix and the X-point). One of our long term goals is the integration of the gyrokinetic turbulence codes in the *core* region (GTC, [10] for example) and in the *edge* region (XGC, [18] for example) (note we do not plan to employ time dependent boundary conditions. Since the gyrokinetic Poisson equation can be solved in the Cartesian coordinate for both core and edge, for the integration purpose, we can employ one field solver). There are a few

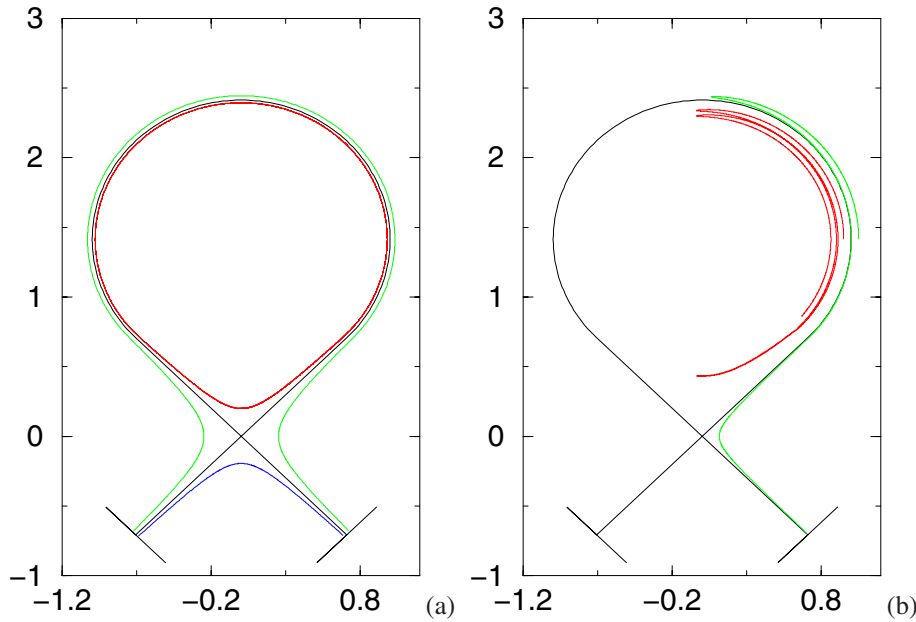


Fig. 2 Guiding center orbit behavior in the Cartesian coordinate system. (a) Guiding center orbit in the absence of toroidal curvature effects ($B = \text{const}$) which is equivalent to magnetic field line Poincare plot. Red plots are for the closed field line, green ones are for the open field line region (corresponds to SOL region), and blue ones are for the private flux region. (b) Trajectories inside and outside separatrix in the presence of toroidal curvature $B_z = B_0(1 - \varepsilon x)$. The initial position of the particles are set at $(x, y) = (0.95, \sqrt{2})$ (red) and $(x, y) = (1.05, \sqrt{2})$ (green). Ion energy of $3.5(\text{keV})$ and the pitch angle scattering operator with $\nu/\Omega_c = 10^{-4}$ are employed. In (a) and (b), the solid black lines and curves represent the separatrix and the divertor plates. (Online colour: www.cpp-journal.org.)

anticipated technical difficulties to overcome. Guiding center variables and the weight function of δf gyrokinetic simulations need to be mapped from one to the other when the particles cross the separatrix. One needs to smoothly connect the effect of collisions with the pitch angle scattering operators conserving the energy. A similar effort is required for the background plasma parameters (the ion and electron temperature gradients η_i , η_e , or T_e/T_i ratio, for example). We also plan to employ Solov'ev solution for the test. [26] We examine these latter issues by employing the orbit following codes presented in this paper.

Acknowledgements This work is supported by Department of Energy (DOE) Cooperative Agreement No. DE-FC02-08ER54957, Grant No. DE-FC02-06ER54860, DE-FC02-08ER54949 and in part by SciDAC Center for Gyrokinetic Particle Simulation of Turbulent Transport in Burning Plasmas and Center for Plasma Edge Simulations.

A Guiding center equation of motion in the Cartesian coordinate

Normalizing Eqs.(4) and (5) by minor radius and ion cyclotron frequency Ω_c , and employing the magnetic field configuration of Eq.(3), the guiding center equation of motion in the Cartesian coordinate system can be written in a simple form (the quantities below are normalized):

$$\dot{x} = v_{\parallel} b_x, \quad (8)$$

$$\dot{y} = v_{\parallel} b_y - \mu \varepsilon b_z, \quad (9)$$

$$\dot{z} = v_{\parallel} b_z + \mu \varepsilon b_y, \quad (10)$$

$$\dot{v}_{\parallel} = \mu \varepsilon b_x. \quad (11)$$

Here, $|B| = B_0(1 - \varepsilon x)$ is employed. In Eqs.(8)-(11), the curvature drift term (on the order of ε^2) is neglected. The electric field is set to be zero. When we employ Eq.(3), the magnitude of the Banos drift [21] is on the order of ε^2 .

References

- [1] F. Wagner et al., Phys. Rev. Lett. **49**, 1408 (1982).
- [2] B. Scott, Phys. Plasmas **7**, 1845 (2000).
- [3] X.Q. Xu, R.H. Cohen, T.D. Rognlien, and J.R. Myra, Phys. Plasmas **7**, 1951 (2000).
- [4] K.C. Shaing and E.C. Crume, Phys. Rev. Lett **63**, 2369 (1989).
- [5] P.H. Diamond and Y.-B. Kim, Phys. Fluids B **3**, 1626 (1991).
- [6] T.D. Rognlien, D. D. Rytov, N. Mattor, and G. D. Porter, Phys. Plasmas **6**, 1851 (1999).
- [7] V. Rozhansky et al., Nucl. Fusion **41**, 387 (2001).
- [8] Y. Nishimura, D. Coster, and B. Scott, Phys. Plasmas **11**, 115 (2004).
- [9] B. Scott, Phys. Plasmas **5**, 2334 (1998).
- [10] Z. Lin, T. S. Hahm, W.W. Lee, W.M. Tang, and R.B. White, Science **281**, 1835 (1998).
- [11] Y. Nishimura, Z. Lin, J.L. V. Lewandowski, and S. Ethier, J. Comput. Phys. **214**, 657 (2006).
- [12] Y. Nishimura and Z. Lin, Contrib. Plasma Phys. **46**, 551 (2006).
- [13] W.W. Lee, J. Comput. Phys. **72**, 243 (1987).
- [14] Z. Lin and W. W. Lee, Phys. Rev. E **52**, 5646 (1995).
- [15] A.H. Boozer, Phys. Fluids **25**, 520 (1982).
- [16] K. Tani, M. Azumi, H. Kishimoto, and S. Tamura, J. Phys. Soc. Japan **50**, 1726 (1981).
- [17] J.A. Heikkinen et al., J. Comput. Phys. **173**, 527 (2001).
- [18] C.S. Chang, S. Kue, and H. Weitzner, Phys. Plasmas **9**, 3884 (2002).
- [19] R.G. Littlejohn, J. Plasma Phys. **29**, 111 (1983).
- [20] A. Brizard, J. Plasma Phys. **41**, 541 (1989).
- [21] A. Banos, J. Plasma Phys. **1**, 305 (1967).
- [22] A.H. Boozer and G. Kuo-Petravic, Phys. Fluids **24**, 851 (1981).
- [23] Y. Nishimura and M. Azumi, Phys. Plasmas **4**, 2365 (1997).
- [24] M. Abramowitz, and I.A. Stegun, *Handbook of Mathematical Functions with Formulas, Graphs, and Mathematical Tables*, (Dover, New York, 1972), p. 896.
- [25] I. Kawakami, *Suuchi-keisan*, (Iwanami, Tokyo, 1989), p. 159 (in Japanese).
- [26] L.S. Solov'ev, Sov. Phys. JETP **26**, 400 (1968).